AGU PUBLICATIONS

Geophysical Research Letters

RESEARCH LETTER
10.1002/2016GL068668

Key Points:
- We present direct high-resolution, months-long measurements of methane venting from lake sediments
- We show that gas vents are ephemeral and not persistent as previously assumed
- Our study provides an unprecedented detailed view of the spatiotemporal signature of methane flux

Supporting Information:
- Supporting Information S1

Correspondence to:
R. Juanes,
juanes@mit.edu

Citation:
Scandella, B. P., L. Pillsbury, T. Weber, C. Ruppel, H. F. Hemond, and R. Juanes (2016), Ephemerality of discrete methane vents in lake sediments, *Geophys. Res. Lett.*, *43*, 4374–4381, doi:10.1002/2016GL068668.

Received 14 MAR 2016
Accepted 28 MAR 2016
Accepted article online 1 APR 2016
Published online 4 MAY 2016

Ephemerality of discrete methane vents in lake sediments

Benjamin P. Scandella[1], Liam Pillsbury[2], Thomas Weber[2], Carolyn Ruppel[3,4], Harold F. Hemond[1], and Ruben Juanes[1,4]

[1]Department of Civil and Environmental Engineering, Massachusetts Institute of Technology, Cambridge, Massachusetts, USA, [2]Department of Mechanical Engineering, University of New Hampshire, Durham, New Hampshire, USA, [3]U.S. Geological Survey, Woods Hole, Massachusetts, USA, [4]Department of Earth, Atmospheric and Planetary Sciences, Massachusetts Institute of Technology, Cambridge, Massachusetts, USA

Abstract Methane is a potent greenhouse gas whose emission from sediments in inland waters and shallow oceans may both contribute to global warming and be exacerbated by it. The fraction of methane emitted by sediments that bypasses dissolution in the water column and reaches the atmosphere as bubbles depends on the mode and spatiotemporal characteristics of venting from the sediments. Earlier studies have concluded that hot spots—persistent, high-flux vents—dominate the regional ebullitive flux from submerged sediments. Here the spatial structure, persistence, and variability in the intensity of methane venting are analyzed using a high-resolution multibeam sonar record acquired at the bottom of a lake during multiple deployments over a 9 month period. We confirm that ebullition is strongly episodic, with distinct regimes of high flux and low flux largely controlled by changes in hydrostatic pressure. Our analysis shows that the spatial pattern of ebullition becomes homogeneous at the sonar's resolution over time scales of hours (for high-flux periods) or days (for low-flux periods), demonstrating that vents are ephemeral rather than persistent, and suggesting that long-term, lake-wide ebullition dynamics may be modeled without resolving the fine-scale spatial structure of venting.

1. Introduction

Emissions from submerged sediments in lakes, rivers, wetlands, and oceans contribute to atmospheric methane, but the nature and magnitude of the release remain uncertain. Owing to their buoyancy and high methane content, bubbles emitted from the sediment transport methane more efficiently than waters containing dissolved methane, and field studies suggest that ebullition is often the dominant mode of methane transfer to the atmosphere [*Martens and val Klump*, 1980; *Kuipphet and Martens*, 1982; *Keller and Stallard*, 1994; *Bastviken et al.*, 2004; *Walter et al.*, 2006; *Bastviken et al.*, 2011; *Maeck et al.*, 2013a]. Ebullitive emissions are episodic and spatially heterogeneous, which complicates upscaling of flux estimates [*Greinert*, 2008; *Ostrovsky et al.*, 2008; *Greinert et al.*, 2010; *DelSontro et al.*, 2011; *Wik et al.*, 2011; *Maeck et al.*, 2013b; *Walter Anthony and Anthony*, 2013; *Wik et al.*, 2013; *DelSontro et al.*, 2015].

The episodicity of methane venting may be driven by either the methane source or an external forcing, depending on which operates on a faster time scale [*Maeck et al.*, 2013b]. For example, drops in hydrostatic or atmospheric pressure trigger ebullition from methane-generating lake sediments [*Scandella et al.*, 2011] and marine sediments [*Martens and val Klump*, 1980; *Kuipphet and Martens*, 1982; *Chanton et al.*, 1989], possibly even in the presence of methane hydrates [*Torres et al.*, 2002]. Spatial heterogeneity in methane venting often manifests as hyperactive vents or vent clusters, sometimes referred to as hot spots [*Walter et al.*, 2006; *Wik et al.*, 2011; *DelSontro et al.*, 2015]. These focused release points may be associated with enhanced microbial methanogenesis [*Ostrovsky et al.*, 2008; *DelSontro et al.*, 2011; *Maeck et al.*, 2013a; *Wik et al.*, 2013], sediment morphological features like pockmarks [*Bussmann et al.*, 2011], a geologic source [*Walter Anthony et al.*, 2012], dissociating gas hydrates [*Westbrook et al.*, 2009; *Berndt et al.*, 2014; *Skarke et al.*, 2014], or rapidly degrading permafrost [*Shakhova et al.*, 2014]. The persistence of bubble outlets and the spacing and variability between them can potentially be used to distinguish the mechanisms controlling ebullition [*Greinert*, 2008; *Wik et al.*, 2011], but observations of these critical parameters are sparse and inconclusive.

Ebullitive fluxes are sometimes measured using bubble traps deployed at discrete locations over an extended time period, but capturing hot spot ebullition or the episodicity of venting events can be challenging with this approach [*Walter et al.*, 2006; *Varadharajan and Hemond*, 2012; *Maeck et al.*, 2013b; *Walter Anthony and Anthony*, 2013; *Wik et al.*, 2013]. Hydroacoustic surveys from ships [*Ostrovsky et al.*, 2008; *Greinert et al.*, 2010;

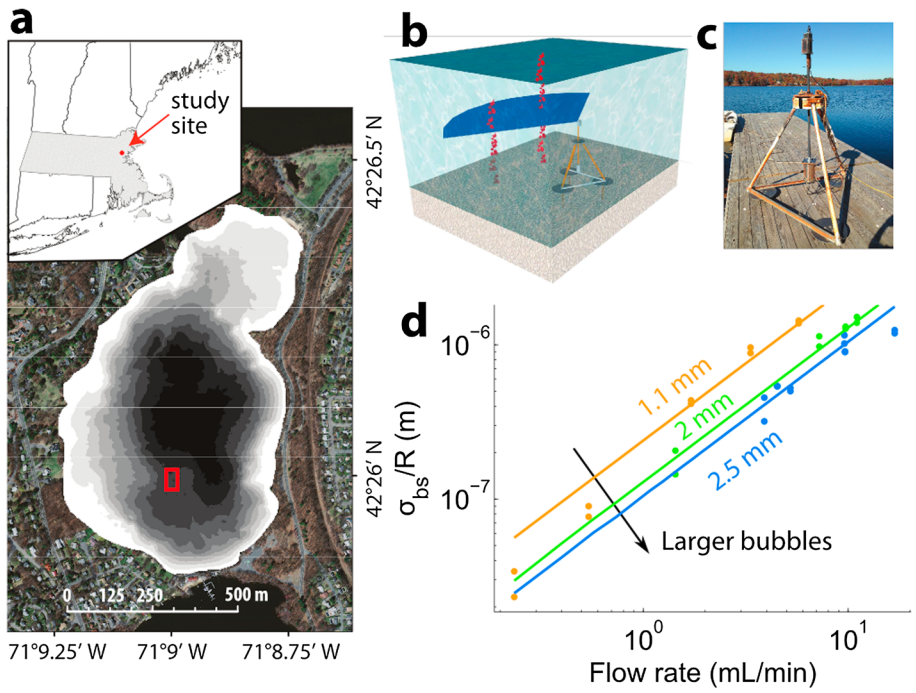

Figure 1. Study area, sonar lander, and calibration. (a) Location of Upper Mystic Lake (inset, Massachusetts, USA shaded) and bathymetry at 2.5 m shaded intervals superposed on an aerial photomosaic. Red square indicates the region bounding the deployment locations (see supporting information). (b) Diagram showing streams of bubbles (red) rising through the horizontally oriented multibeam sonar fan (blue, not to scale). (c) Photo of the deployment tripod before redeployment. (d) Calibration curves over 2 orders of magnitude in gas flow rate and for three different bubble size classes. Data points represent the time-averaged sonar response to streams of a given flow rate, and lines indicate modeled responses for each bubble class (radius in millimeter, see supporting information).

DelSontro et al., 2011, 2015; *Skarke et al.*, 2014; *Weber et al.*, 2014] cover large areas but only at discrete times and therefore cannot be used for continuously quantifying fluxes. Short- and long-term seafloor deployments of hydroacoustic sensors [*Greinert*, 2008] can detect ebullitive events at specific locations but require careful calibration to infer spatially resolved fluxes. Here we extend the hydroacoustic approach to acquire long-term, high-resolution methane emission records from a lake bottom to test hypotheses about the driving forces for ebullition events and the mechanisms controlling spacing and persistence of gas vents.

2. Multibeam Sonar Deployment

An Imagenex 837B DeltaT 260 kHz rotating multibeam sonar was deployed on a benthic lander in the deep-water basin (18–19 m) of Upper Mystic Lake (UML), an eutrophic kettle lake north of Boston, MA (Figure 1). The sonar surveyed in a horizontal plane ≈1.5 m above the lake's bottom and ≈8–9 m below the depth of observed thermoclines to collect data over a 9 month period in a ≈330 m^2 area. The sediments within this region are organic rich (20–40%) [*Spliethoff and Hemond*, 1996] and remain anoxic and at roughly constant temperature beneath the 4–6°C hypolimnetic water [*Varadharajan*, 2009]. The previously measured sediment accumulation rate of 0.5 cm/yr is expected to be homogeneous within the basin due to relatively flat bathymetry, and freeze cores from within the basin show strikingly similar depth profiles of arsenic concentration [*Spliethoff and Hemond*, 1996]. Over the scale of the lake, deposition rates are expected to be faster near the periphery and the northern end, where water flows in from a forebay. An identical sonar was calibrated in a 1300 m^3 freshwater tank at the University of New Hampshire to convert the sonar signals into estimates of the instantaneous flow rate from bubble streams (Figure 1d), which were then integrated to calculate the flux associated with ebullition episodes (see Methods and supporting information).

3. Temporal Signature of Methane Venting

Episodicity observed in spatially averaged daily flux from the sonar data confirms that strong venting episodes can be triggered by drops in hydrostatic pressure (Figure 2a), although the negative correlation of ebullition

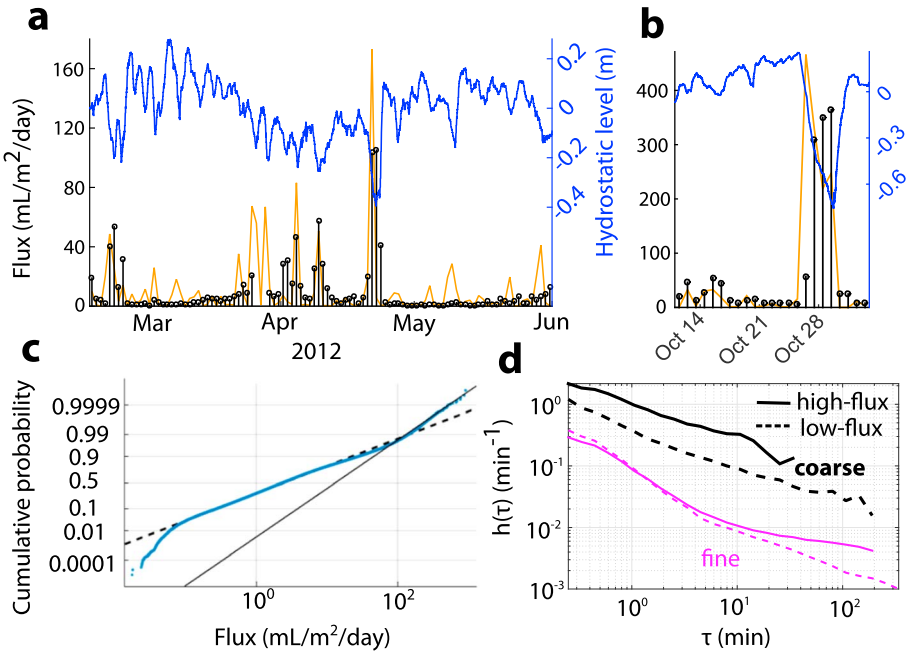

Figure 2. Episodicity of methane venting. (a) Time series of daily, spatially averaged fluxes (black bars) from 10 February through 31 May 2012 shows that enhanced fluxes are triggered by hydrostatic pressure drops (blue line). The episodicity of this triggering can be reproduced using a mechanistic numerical model of gas release through dynamic conduits (orange line). (b) Time series from October 2012, when a hydrostatic pressure drop of 1 m beginning on 26 October triggered massive venting (note the different axis scales) at a different location from the data presented in Figure 2a (see supporting information). (c) Cumulative distribution of 1 min spatially averaged flux values shows three distinct lognormal regimes, which each appears as lines of constant slope on the given axes. (d) The hazard function h decays as a power law with interarrival time τ for coarse (64 m^2, black) and fine (0.25 m^2, red) pixels during high-flux (solid lines) and low-flux (dashed lines) periods.

rate with hydrostatic pressure and its rate of change ($R^2 = 0.5$ and 0.1, respectively) is weak, primarily because not all hydrostatic pressure drops trigger ebullition episodes. For example, the releases in late February and late April 2012 are both followed by month-long periods of relative quiescence, despite several ≈0.3 m hydrostatic drops that had earlier been enough to trigger large methane releases. The duration of these quiescent periods reflects the time for sediments to recharge the trapped bubbles to a size large enough to be susceptible to mobilization by hydrostatic triggering.

Hydrostatic triggering of ebullition may be explained mechanistically as a response to changes in effective stress. With falling hydrostatic pressure, total stress is reduced, forcing gas-charged sediments into a more tensile effective stress state. At a critical stress, gas-filled cavities then dilate near-vertical conduits to the sediment's surface [*Boudreau et al.*, 2005; *Jain and Juanes*, 2009], and the critical stress may be modeled assuming that the sediment-water matrix is elastic [*Algar et al.*, 2011a, 2011b] or plastic [*Scandella et al.*, 2011]. The timing and relative magnitude of many of the peak ebullition events can be reproduced using a numerical model [*Scandella et al.*, 2011] that captures this process and that is tuned with another UML data set (Figures 2a and 2b). The tuning parameter, the ebullition number, controls the episodicity of methane fluxes and reflects the balance between the tensile strength of the sediment-water matrix and the characteristic hydrostatic pressure variations. The model can capture the features of most large ebullition events, although it does not fully reproduce the long quiescent periods during March and May 2012 (Figures 2a and 2b).

The high temporal resolution, together with the large areal coverage and long duration of the sonar record, allows for a more detailed analysis of ebullition dynamics that had previously been possible with bubble-trap methods. High-frequency flux measurements (binned at 1 min) show that approximately 98% of the flux measurements follow a lognormal distribution over 3 orders of magnitude (0.1–100 mL/m^2/d) (Figure 2c, see supporting information). Lognormally distributed measurements typically arise from processes controlled by the product of independent factors, which in this setting may include the bubble mobilization rate over the observation area and heterogeneity in conductivity of dynamic gas escape pathways.

Further insight into processes controlling ebullition is furnished by the distribution of interarrival times between bubble-release events—"events" are bubble-release sequences that persist with breaks no longer than 2 s (given 5 s moving-average filtering). Distributions of interarrival times may be analyzed using the hazard function

$$h(\tau) = \frac{f(\tau)}{1 - F(\tau)}, \quad (1)$$

where $f(\tau)$ is the probability density function of interarrival times τ, and $F(\tau)$ is the cumulative density function [*Stapelberg*, 2009]. $h(\tau)$ quantifies the probability of an event occurring conditioned on a given amount of time having passed since the last event. For a Poisson process, events are independent and have uniform probability, corresponding to constant h since the events have no memory of previous arrivals. For a Weibull process—a model often used in reliability engineering to model component failures—the hazard function is a power law, $h(\tau) = (\beta/\lambda)(\tau/\lambda)^{\beta-1}$, where β and λ are the shape and scale parameters, respectively. A decreasing power law ($\beta < 1$) corresponds to strong temporal clustering, while an increasing power law ($\beta > 1$) is associated with more regularly periodic arrivals [*Stapelberg*, 2009].

In UML, ebullition events are characterized by decaying power laws. For events collected from a 64 m^2 averaging area, the decay in both high- and low-flux regimes is well fit by $\beta \approx 0.4$, which reflects mild temporal clustering (Figure 2d). At the fine-scale resolution of the sonar (0.25 m^2), $h(\tau)$ shows two distinct regimes characterized by different power law scalings. For short-term interarrival times ($\tau < 5$ min), the decay has a slope less than −1, indicating stronger short-term clustering than possible with a Weibull process, which requires $\beta > 0$. The power law regime does not extend over all τ but instead transitions to a regime of more gradual decay over long interarrival times ($\tau > 5$ min), consistent with reestablishment of sediment cohesion and healing of vent conduits. Over long τ, the high-flux regime shows even more gradual decay in $h(\tau)$ than the low-flux regime, implying a larger role for independent arrivals.

4. Spatial Signature of Methane Venting

The spatial structure of methane venting is found to depend on the overall flux regime (high flux versus low flux). Daily gas flux maps during high-flux periods reveal gas release from densely spaced outlets, while the low-flux periods are associated with sparser venting (Figure 3a). The ubiquity of venting across the observation area during high-flux periods may reflect the relative homogeneity of methanogenesis, whose controlling parameters (sediment accumulation and temperature) are fairly homogeneous above the meter scale in the deepwater basin [*Spliethoff and Hemond*, 1996].

During high-flux periods, ebullition events occur in clusters of enhanced activity, although, over time, events appear throughout the field of observation. While some locations vent gas at over 3 times the spatiotemporal mean flux of 10 mL/m^2/d (Figure 3b), these contribute only 1% of the total flux, suggesting a minimal role for hot spots. Instead, gas appears to be released through independent, near-vertical conduits or conduit networks linked to outlets, where the scale of lateral transport or significant heterogeneity in sediment properties is less than the resolution of the sonar, 0.5 m. Such a laterally dense network of release pathways should develop in sediments that generate methane throughout their bulk. In this case, transport from the sediment matrix toward release pathways would be diffusion limited to a distance on the scale of centimeters in the days to weeks between ebullition events. The outlet and conduit spacing may also be controlled by heterogeneity in the chemistry and mechanics of the sediments, though our results show that such heterogeneity does not give rise to persistent outlets spaced more than 0.5 m apart.

A spatial clustering analysis of the observed methane-flux signal yields additional clues about the system's self-organization. Our analysis is based on the radial distribution function (RDF), $g(r)$, which detects clustering as a function of interpoint distance r [*Illian et al.*, 2008] (see Methods and supporting information). The analysis yields $g > 1$ for short-range ($r < 1$ m) events over short time periods (10 min and 1 h samples), indicating a high areal density of events relative to a completely spatially random (CSR) process. The short-range clustering is balanced by long-range spacing ($g < 1$ for $r > 1$ m). This signature of short-range clustering and long-range spacing was strongest for 10 min samples and became progressively weaker for longer duration samples, eventually decaying to a homogeneous RDF ($g(r) \approx 1$) over daily samples (Figure 3d). This clustering signature indicates that gas is vented from nearby, distinct outlets within a short period of time (see Methods and supporting information).

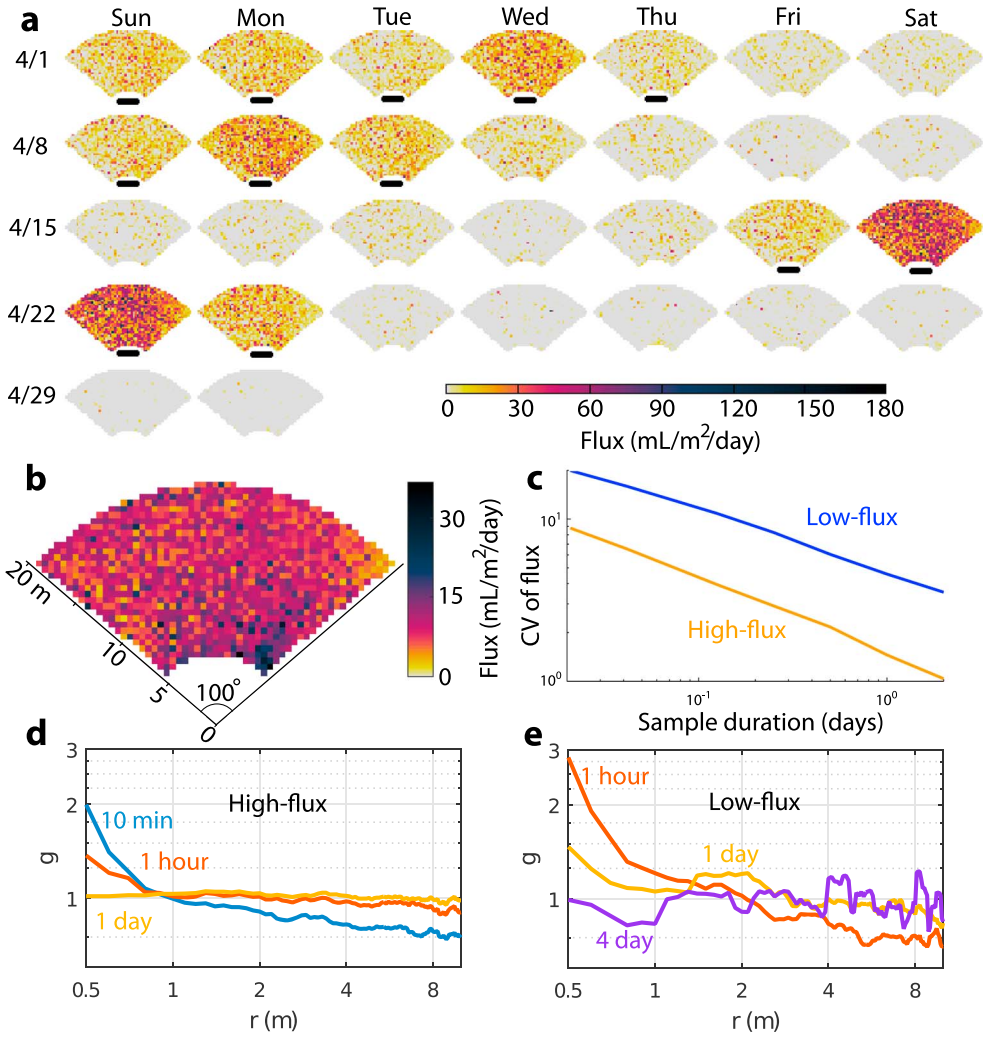

Figure 3. Spatial structure of methane venting. (a) This calendar representation of daily sonar-detected gas venting in April 2012 shows the spatial variability of methane fluxes across the sonar detection area. Days with higher than average flux are underlined. (b) Average flux map from March to May 2012. (c) Spatial coefficient of variation (CV) between flux measurements on a grid with resolution of 0.5 m, averaged over samples of duration 1–24 h collected during Spring 2012. (d and e) Radial distribution function (RDF), $g(r)$, for high-flux (Figure 3d) and low-flux (Figure 3e) periods during Spring 2012.

Compared with the high-flux regime, low-flux periods show both stronger variability and longer persistence in the structure of the heterogeneity. For a given observation duration, the coefficient of variation (CV) across space is more than twice the CV from high-flux periods (Figure 3c). The spatial structure of this variability is evident in the RDF, which exhibits short-range spatial clustering that is similar to the clustering observed during high-flux periods, except that it extends to $r \leq 2$ m and persists over timescales as long as 1 day (Figure 3e, see supporting information).

The ephemeral nature of spatial clustering evidenced by the RDF is consistent with the spatial localization of short-term temporal clustering observed in $h(\tau)$ and is likely associated with the same process. Ebullition events may trigger "aftershock" events by mechanically disturbing nearby sediments that contain critically stressed gas pockets. Due to the compliance of the sediments and the small magnitude of deformation associated with bubble passage, this mechanism would likely require that trapped bubbles be spaced only a few centimeters apart.

The decay of clustering over progressively longer periods indicates that individual outlet clusters are active for a short time but do not persist to dominate the long-term flux pattern. Instead, independent outlets or clusters subsequently become active at intermediate, independent locations until the domain is filled with

emission sites approximating a CSR pattern. The clustering pattern in the RDF decays faster during high-flux periods, suggesting that higher fluxes arise primarily from more frequent initiation of spatially independent events. The spatial independence of new arrivals over long time periods is consistent with the conceptual model that long-term, large-scale fluxes are driven by hydrostatic pressure drops, which act equally over the sediment surface to liberate trapped gas.

5. Conclusions

In summary, the high spatial and temporal resolution afforded by the sonar data allows discernment of discrete ebullitive episodes and vent locations, and the long deployments permit analyses over months' long periods. Our analysis shows that specific methane vents in UML do not repeatedly dominate fluxes during ebullitive episodes; instead, vents are frequently forming and closing off throughout the homogeneous sediments that make up the seep field in the lake's deep basin. This finding challenges the idea that sediment vents, once established, will continue to be the preferential loci over the scale of meters. While these results may not directly apply to settings with more heterogeneous geology [*Hornbach et al.*, 2004; *Walter Anthony et al.*, 2012; *Skarke et al.*, 2014] or sediment deposition patterns [*Bussmann et al.*, 2011; *DelSontro et al.*, 2011; *Maeck et al.*, 2013a; *DelSontro et al.*, 2015], they suggest that the acquisition of longer and more spatially comprehensive data sets on ebullition events in such settings may better constrain the relative importance of hot spot versus distributed methane emissions from submerged sediments for both local and global flux estimates.

Appendix A: Methods Summary

A1. Sonar

The sonar data were acquired using an Imagenex 837B multibeam profiling sonar, which detects acoustic targets with high spatial and temporal resolution over a roughly planar observation area, a fan of ≈100° by ≈2°. The pulse repetition rate was approximately 6 Hz so that bubbles at 1 and 20 m range were insonified by 1 and 30 consecutive pings, respectively. The locations of the detected bubbles are accurate to <0.5 m because the distance resolution was 0.18 m and the angular resolution of 1° corresponds to at most 0.4 m at the maximum range of 20 m. The horizontal orientation of the unit was set using a gimbal and measured to remain within ≈0.2° of horizontal with an on-board pitch-roll-heading sensor.

The directional sensitivity of the sonar was corrected using a combination of the beam pattern measured in the ocean engineering tank at the University of New Hampshire (UNH) and tuning to remove large-scale directional sensitivity from the long-term average flux during a given multimonth deployment period (see supporting information).

A2. Calibration

The sonar was calibrated to estimate the volumetric flow rate of bubble streams rising through its observation area of ≈330 m^2. The calibration was performed on a unit of the same model in the Ocean Engineering tank at UNH by injecting bubbles at a constant flow rate and bubble size distribution from beneath the sonar fan. The bubble sizes were measured independently using a camera in a waterproof housing, and the rate of bubble release was monitored with a passive hydrophone. The time-averaged backscatter $\overline{\sigma}_{bs}$ measured by the sonar scaled linearly with the flow rate Q at a given bubble size, and the calibration coefficient K varied with the bubble size (Figure 1d),

$$Q = K\left(\frac{\overline{\sigma}_{bs}}{R}\right), \tag{A1}$$

where R is the range, the distance from the sonar head to the target. The dependence on flow rate and bubble size matched predictions from an analytical model of the expected sonar response to a constant bubble stream rising through a horizontally oriented multibeam sonar. The expected response from a bubble stream with a wide but constant bubble size distribution was calculated by adapting a method that was developed for single and split beam sonar [*Muyakshin and Sauter*, 2010; *Veloso et al.*, 2015], assuming a constant bubble size distribution measured in UML with an optical bubble sizer [*Delwiche et al.*, 2015] and assuming that plumes are too sparse to be influenced significantly by multiple scatter reflections (see supporting information). The relative uncertainty in flux estimates is estimated to be ~70% (see supporting information).

A3. Bubble Identification

After the raw data were smoothed with a 5 s moving-average filter and coarsened to 1 s resolution, they were thresholded to identify connected groups of pixels contributing a minimum flow rate, 0.03 mL/min. Ebullition events, comprising a series of bubbles released in rapid succession from the same location, were identified from the time series of flow rates from these active groups as periods of nonzero activity with breaks of no more than 2 s. The volume of gas estimated by the sonar was adjusted to STP.

Candidate ebullition events were distinguished from nonbubble targets with limits on their intensity and duration, and this process correctly classified >99% of both the bubble and nonbubble volume (see supporting information).

A4. Hazard Function

The hazard function was estimated using a histogram of the event interarrival times to estimate $f(\tau)$, which was then converted to $h(\tau)$ using the definition in equation (1). Logarithmically spaced bins were used to reduce the variance of the estimator at long interarrival times, and the estimator was validated with simulations of Poisson and Weibull processes. A minimum interarrival time of 15 s was used because this represents the characteristic duration of bubbling events. In order to analyze long, continuous records in each location, day-long samples were classified as either high flux or low flux based on their relation to the long-term average flux, which is independent of the time scale of coarsening.

A5. Radial Distribution Function

To account for the enhanced importance of events releasing large volumes of gas, the volume-weighted RDF $g(r)$ was estimated using the marked pair correlation function [*Illian et al.*, 2008] (see supporting information). Estimating the RDF requires an observation window within which the data are first-order stationary in density and magnitude [*Illian et al.*, 2008]. This stationary window was found to span the central 60° of the sonar fan and from 6 to 20 m from the sonar head (Figure 3b), after correcting for the directional sensitivity of the sonar.

A6. Conduit Dilation Model

The episodicity of spatially-averaged fluxes was reproduced with a numerical, mechanistic model of methane gas transport through dynamic conduits that dilate in response to changes in effective stress [*Scandella et al.*, 2011]. This 1-D model captures the accumulation of trapped gas in a vertical column of sediment and tracks the gas pressure and volume as a hydrostatic pressure forcing triggers plastic deformation of the sediment-water matrix surrounding gas cavities. When the effective stress reaches a depth-dependent tensile strength threshold, the gas forces open a conduit to the surface and escape. The fundamental parameter of the model, called the ebullition number, N_e, reflects the balance between the vertical gradient in tensile strength of the mud and the characteristic magnitude of hydrostatic pressure changes. Larger values of N_e require larger, rarer drops in hydrostatic pressure to release gas from the deepest sediments and thus drive more strongly episodic venting. In this study, the best fit value of $N_e = 5$ was the same as in a previous study on UML that quantified ebullition with floating bubble traps [*Scandella et al.*, 2011].

Acknowledgments

We thank Kyle Delwiche, Hannah Wood and Jared Darby of MIT, W. Baldwin, D. Blackwood and the USGS Woods hole technical and operational group, Carlo Lanzoni of UNH, Jens Greinert of GEOMAR, Doug Wilson and the Imagenex Technology Corporation, Coach Kenneth Legler and the Tufts Sailing Team, and the Winchester Boat Club. This work was supported by the U.S. National Science Foundation (award 1045193) and the U.S. Department of Energy (grant DE-FE0013999). Any use of a trade, product, or firm name is for descriptive purposes only and does not imply endorsement by the U.S. Government.

References

Algar, C. K., B. P. Boudreau, and M. A. Barry (2011a), Initial rise of bubbles in cohesive sediments by a process of viscoelastic fracture, *J. Geophys. Res.*, *116*, B04207, doi:10.1029/2010JB008133.

Algar, C. K., B. P. Boudreau, and M. A. Barry (2011b), Release of multiple bubbles from cohesive sediments, *Geophys. Res. Lett.*, *38*, L08606, doi:10.1029/2011GL046870.

Bastviken, D., J. Cole, M. Pace, and L. Tranvik (2004), Methane emissions from lakes: Dependence of lake characteristics, two regional assessments, and a global estimate, *Global Biogeochem. Cycles*, *18*, GB4009, doi:10.1029/2004GB002238.

Bastviken, D., L. J. Tranvik, J. A. Downing, P. M. Crill, and A. Enrich-Prast (2011), Freshwater methane emissions offset the continental carbon sink, *Science*, *331*, 50.

Berndt, C., et al. (2014), Temporal constraints on hydrate-controlled methane seepage off Svalbard, *Science*, *343*(6168), 284–287.

Boudreau, B., C. Algar, B. Johnson, I. Croudace, A. Reed, Y. Furukawa, K. Dorgan, P. Jumars, A. Grader, and B. Gardiner (2005), Bubble growth and rise in soft sediments, *Geology*, *33*(6), 517–520.

Bussmann, I., S. Schlomer, M. Schluter, and M. Wessels (2011), Active pockmarks in a large lake (Lake Constance, Germany): Effects on methane distribution and turnover in the sediment, *Limnol. Oceanogr.*, *56*(1), 379–393.

Chanton, J., C. Martens, and C. Kelley (1989), Gas transport from methane-saturated, tidal freshwater and wetland sediments, *Limnol. Oceanogr.*, *34*(5), 807–819.

DelSontro, T., M. J. Kunz, T. Kempter, A. Wueest, B. Wehrli, and D. B. Senn (2011), Spatial heterogeneity of methane ebullition in a large tropical reservoir, *Environ. Sci. Technol.*, *45*(23), 9866–9873.

DelSontro, T., D. F. McGinnis, B. Wehrli, and I. Ostrovsky (2015), Size does matter: Importance of large bubbles and small-scale hot spots for methane transport, *Environ. Sci. Technol.*, *49*(3), 1268–1276.

Delwiche, K., S. Senft-Grupp, and H. Hemond (2015), A novel optical sensor designed to measure methane bubble sizes in situ, *Limnol. Oceanogr.*, *13*, 712.

Greinert, J. (2008), Monitoring temporal variability of bubble release at seeps: The hydroacoustic swath system GasQuant, *J. Geophys. Res.*, *113*, C07048, doi:10.1029/2007JC004704.
Greinert, J., D. F. McGinnis, L. Naudts, P. Linke, and M. De Batist (2010), Atmospheric methane flux from bubbling seeps: Spatially extrapolated quantification from a Black Sea shelf area, *J. Geophys. Res.*, *115*, C01002, doi:10.1029/2009JC005381.
Hornbach, M., D. Saffer, and W. Holbrook (2004), Critically pressured free-gas reservoirs below gas-hydrate provinces, *Nature*, *427*(6970), 142–144.
Illian, J., A. Penttinen, H. Stoyan, and D. Stoyan (2008), *Statistical Analysis and Modelling of Spatial Point Patterns*, Wiley, West Sussex, England.
Jain, A. K., and R. Juanes (2009), Preferential mode of gas invasion in sediments: Grain-scale mechanistic model of coupled multiphase fluid flow and sediment mechanics, *J. Geophys. Res.*, *114*, B08101, doi:10.1029/2008JB006002.
Keller, M., and R. Stallard (1994), Methane emission by bubbling from Gatun Lake, Panama, *J. Geophys. Res.*, *99*(D4), 8307–8319.
Kuipphet, G., and C. Martens (1982), Biogeochemical cycling in an organic-rich coastal marine basin. 3. Dissolved gas transport in methane-saturated sediments, *Geochim. Cosmochim. Acta*, *46*(11), 2049–2060.
Maeck, A., T. DelSontro, D. F. McGinnis, H. Fischer, S. Flury, M. Schmidt, P. Fietzek, and A. Lorke (2013a), Sediment trapping by dams creates methane emission hot spots, *Environ. Sci. Technol.*, *47*(15), 8130–8137.
Maeck, A., H. Hofmann, and A. Lorke (2013b), Pumping methane out of aquatic sediments; forcing mechanisms that affect the temporal dynamics of ebullition, *Biogeosci. Discuss.*, *10*(11), 18,687–18,722.
Martens, C., and J. val Klump (1980), Biogeochemical cycling in an organic-rich coastal marine basin. 1. Methane sediment-water exchange processes, *Geochim. Cosmochim. Acta*, *44*(3), 471–490.
Muyakshin, S. I., and E. Sauter (2010), The hydroacoustic method for the quantification of the gas flux from a submersed bubble plume, *Oceanology*, *50*(6), 1045–1051.
Ostrovsky, I., D. F. McGinnis, L. Lapidus, and W. Eckert (2008), Quantifying gas ebullition with echosounder: The role of methane transport by bubbles in a medium-sized lake, *Limnol. Oceanogr.*, *6*, 105–118.
Scandella, B. P., C. Varadharajan, H. F. Hemond, C. Ruppel, and R. Juanes (2011), A conduit dilation model of methane venting from lake sediments, *Geophys. Res. Lett.*, *38*, L06408, doi:10.1029/2011GL046768.
Shakhova, N., et al. (2014), Ebullition and storm-induced methane release from the East Siberian Arctic Shelf, *Nat. Geosci.*, *7*(1), 64–70.
Skarke, A. D., C. D. Ruppel, M. Kodis, D. Brothers, and E. Lobecker (2014), Widespread methane leakage from the sea floor on the northern US Atlantic margin, *Nat. Geosci.*, *7*(9), 657–661.
Spliethoff, H., and H. Hemond (1996), History of toxic metal discharge to surface waters of the Aberjona Watershed, *Environ. Sci. Technol.*, *30*(1), 121–128.
Stapelberg, R. F. (2009), *Handbook of Reliability, Availability, Maintainability and Safety in Engineering Design*, Springer, London.
Torres, M., J. McManus, D. Hammond, M. de Angelis, K. Heeschen, S. Colbert, M. Tryon, K. Brown, and E. Suess (2002), Fluid and chemical fluxes in and out of sediments hosting methane hydrate deposits on Hydrate Ridge, OR, I: Hydrological provinces, *Earth Planet. Sci. Lett.*, *201*(3–4), 525–540.
Varadharajan, C. (2009), Magnitude and spatio-temporal variability of methane emissions from a eutrophic freshwater lake, PhD Thesis, Massachusetts Inst. of Technol., Cambridge, Mass.
Varadharajan, C., and H. F. Hemond (2012), Time-series analysis of high-resolution ebullition fluxes from a stratified, freshwater lake, *J. Geophys. Res.*, *117*, G02004.
Veloso, M., J. Greinert, J. Mienert, and M. De Batist (2015), A new methodology for quantifying bubble flow rates in deep water using splitbeam echosounders: Examples from the Arctic offshore NW-Svalbard, *Limnol. Oceanogr. Methods*, *13*(6), 267–287.
Walter, K. M., S. A. Zimov, J. P. Chanton, D. Verbyla, and F. S. Chapin III (2006), Methane bubbling from Siberian thaw lakes as a positive feedback to climate warming, *Nature*, *443*, 71–75.
Walter Anthony, K. M., and P. Anthony (2013), Constraining spatial variability of methane ebullition seeps in thermokarst lakes using point process models, *J. Geophys. Res.*, *118*(3), 1015–1034.
Walter Anthony, K. M., P. Anthony, G. Grosse, and J. Chanton (2012), Geologic methane seeps along boundaries of Arctic permafrost thaw and melting glaciers, *Nat. Geosci.*, *5*, 419–426.
Weber, T. C., L. Mayer, K. Jerram, J. Beaudoin, Y. Rzhanov, and D. Lovalvo (2014), Acoustic estimates of methane gas flux from the seabed in a 6000 km^2 region in the Northern Gulf of Mexico, *Geochem. Geophys. Geosyst.*, *15*(5), 1911–1925.
Westbrook, G. K., et al. (2009), Escape of methane gas from the seabed along the West Spitsbergen continental margin, *Geophys. Res. Lett.*, *36*, L15608, doi:10.1029/2009GL039191.
Wik, M., P. M. Crill, D. Bastviken, A. Danielsson, and E. Norback (2011), Bubbles trapped in arctic lake ice: Potential implications for methane emissions, *J. Geophys. Res.*, *116*, G03044, doi:10.1029/2011JG001761.
Wik, M., P. M. Crill, R. K. Varner, and D. Bastviken (2013), Multiyear measurements of ebullitive methane flux from three subarctic lakes, *J. Geophys. Res. Biogeosci.*, *118*, 1307–1321, doi:10.1002/jgrg.20103.